ORIGINAL ARTICLE

Differentially disrupted functional connectivity of the subregions of the inferior parietal lobule in Alzheimer's disease

Zhiqun Wang · Mingrui Xia · Zhengjia Dai ·
Xia Liang · Haiqing Song · Yong He · Kuncheng Li

Abstract Recent research on Alzheimer's disease (AD) has shown that the altered structure and function of the inferior parietal lobule (IPL) provides a promising indicator of AD. However, little is known about the functional connectivity of the IPL subregions in AD subjects. In this study, we collected resting-state functional magnetic resonance imaging data from 32 AD patients and 38 healthy controls. We defined seven subregions of the IPL according to probabilistic cytoarchitectonic atlases and mapped the whole-brain resting-state functional connectivity for each subregion. Using hierarchical clustering analysis, we identified three distinct functional connectivity patterns of the IPL subregions: the anterior IPL connected with the sensorimotor network (SMN) and salience network (SN); the central IPL had connectivity with the executive-control network (ECN); and the posterior IPL exhibited connections with the default-mode network (DMN). Compared with the controls, the AD patients demonstrated distinct disruptive patterns of the IPL subregional connectivity with these different networks (SMN, SN, ECN and DMN), which suggests the impairment of the functional integration in the IPL. Notably, we also observed that the IPL subregions showed increased connectivity with the posterior part of the DMN in AD patients, which potentially indicates a compensatory mechanism. Finally, these abnormal IPL functional connectivity changes were closely associated with cognitive performance. Collectively, we show that the subregions of the IPL present distinct functional connectivity patterns with various functional networks that are differentially impaired in AD patients. Our results also suggest that functional disconnection and compensation in the IPL may coexist in AD.

Keywords Supramarginal gyrus · Angular gyrus · Network · fMRI · Alzheimer disease

Z. Wang, and M. Xia contributed equally to this work.

Z. Wang · K. Li (✉)
Department of Radiology, Xuanwu Hospital of Capital Medical University, Beijing 100053, China
e-mail: likuncheng@xwh.ccmu.edu.cn

M. Xia · Z. Dai · X. Liang · Y. He (✉)
State Key Laboratory of Cognitive Neuroscience and Learning and IDG/McGovern Institute for Brain Research, Beijing Normal University, Beijing 100875, China
e-mail: yong.he@bnu.edu.cn

M. Xia · Z. Dai · X. Liang · Y. He
Center for Collaboration and Innovation in Brain and Learning Sciences, Beijing Normal University, Beijing 100875, China

H. Song
Department of Neurology, Xuanwu Hospital of Capital Medical University, Beijing 100053, China

K. Li
Key Laboratory for Neurodegenerative Diseases, Capital Medical University, Ministry of Education, Beijing 100069, China

K. Li
Beijing Key Laboratory of Magnetic Resonance Imaging and Brain Informatics, Beijing 100875, China

Introduction

Alzheimer's disease (AD) is characterized by amyloid-β plaques, neurofibrillary tangles and neuronal loss (Braak and Braak 1991). Neuroimaging studies have suggested that these neuropathological changes are closely associated with the disrupted intrinsic resting-state functional connectivity (RSFC) within specific brain systems, which might contribute to memory deficits and cognitive impairment (Seeley et al. 2009; Buckner et al. 2009; Pievani et al. 2011a, b).

Resting-state functional magnetic resonance imaging (R-fMRI), a promising neuroimaging technique that can measure intrinsic neural activity, such as fluctuations in the blood-oxygen level-dependent signals, has been widely used to investigate the RSFCs of the human brain (Biswal et al. 1995; Zhang and Raichle 2010). Many R-fMRI studies have demonstrated that AD patients exhibit abnormal RSFCs in the various brain regions that are targeted by AD pathology, such as the hippocampus (Allen et al. 2007; Wang et al. 2006), posterior cingulate cortex (Greicius et al. 2004; Zhang et al. 2010), prefrontal cortex (Wang et al. 2007; Dai et al. 2012) and thalamus (Wang et al. 2012b). Aside from these regions, the inferior parietal lobule (IPL) has begun to show promise as an important locus in AD (Greene and Killiany 2010). For example, several studies have shown AD-related alterations of the IPL, such as gray matter (GM) atrophy (Desikan et al. 2009; Jacobs et al. 2011), metabolic dysfunction (Walhovd et al. 2010) and pathological changes (Nelson et al. 2009; Braak and Braak 1991). These studies raise the possibility that the IPL RSFCs could be disrupted in AD patients.

The IPL is a heterogeneous area that involves multimodal functions, including sensory motor processing (Iacoboni 2005; Keysers and Gazzola 2009), executive control (Uddin et al. 2011) and salience detection (Seeley et al. 2007). Cytoarchitectonic analyses have suggested that the human IPL can be parcellated into seven subregions, including five regions of the supramarginal gyrus (SMG) and two regions of the angular gyrus (ANG) (Caspers et al. 2006, 2008). Neuroimaging studies have shown different structural and functional connectivity patterns in the IPL subregions (Mars et al. 2011; Wang et al. 2012a). The regions of the SMG are connected with the sensorimotor network (SMN), salience network (SN) and executive control network (ECN), whereas the regions of the ANG are linked with the default-mode network (DMN). Considering the IPL heterogeneity and its association with AD neuropathology, it is important to ascertain the intrinsic RSFC patterns of the IPL subregions in AD. However, no studies have reported AD-related RSFC alterations of the IPL subregions.

Here, we used R-fMRI to investigate the intrinsic functional connectivity of the IPL subregions in AD patients and healthy subjects. We identified seven subregions of the IPL using probabilistic cytoarchitectonic atlases and mapped the whole-brain RSFCs of each subregion, which was followed by a group comparison (see "Materials and methods"). Based on the above-mentioned studies, we sought to determine (1) whether the patients with AD show differentially disrupted RSFC patterns between the SMN, SN, ECN and DMN networks and each IPL subregion and (2) whether these RSFC alterations are associated with behavioral features of AD.

Materials and methods

Participants

Thirty-four patients with AD and forty-one healthy controls (HCs) participated in the study after giving written informed consent. This study was approved by the Medical Research Ethics Committee of Xuanwu Hospital. The data from five subjects (two AD patients and three HCs) were excluded because of a failure in the image processing (see Image preprocessing). Clinical and demographic information for the remaining 70 participants (32 AD patients and 38 HCs) are shown in Table 1. Previously, a subset of this dataset (16 AD patients and 22 HCs) was used to study the changes in regional brain activity in AD (Wang et al. 2011). The AD patients were recruited from individuals who had consulted a memory clinic at Xuanwu Hospital

Table 1 Demographic and neuropsychological test

	AD ($n = 32$)	HC ($n = 38$)	P value
Age (years)	52–86 (71.25 ± 8.63)	50–86 (68.39 ± 7.78)	0.15[a]
Gender (male/female)	14/18	13/25	0.41[b]
CDR	0.5 ($n = 14$), 1 ($n = 18$)	0	–
MMSE	10–25 (18.56 ± 3.99)	28–30 (28.63 ± 0.67)	<0.001[a]
AVLT	8–24 (14.81 ± 4.12)	39–52 (44.42 ± 2.74)	<0.001[a]
ESD	107–200 (155.33 ± 26.48)	180–248 (227.74 ± 15.68)	<0.001[a]
MoCA	8–19 (14.94 ± 3.23)	27–30 (28.63 ± 0.67)	<0.001[a]
CDT	3–8 (6.13 ± 1.43)	8–9 (8.71 ± 0.46)	<0.001[a]
ADL	22–45 (30.41 ± 7.21)	20–22 (21.08 ± 0.78)	<0.001[a]
FAQ	4–11 (6.25 ± 1.70)	0–2 (0.55 ± 0.76)	<0.001[a]
HAMD	0–3 (1.06 ± 1.08)	0–3 (0.61 ± 1.00)	0.07[a]
HIS	0–3 (1.16 ± 0.77)	0–3 (1.13 ± 1.07)	0.91[a]

Data are presented as the range of minimum–maximum (mean ± SD)

AD Alzheimer's disease, *HC* healthy control, *CDR* clinical dementia rating, *MMSE* mini-mental state examination, *AVLT* World Health Organization–University of California–Los Angeles auditory verbal learning test, *ESD* The Extended Scale for Dementia, *MoCA* montreal cognitive assessment, *CDT* clock drawing task, *ADL* Activity of Daily Living Scale, *FAQ* Functional Activities Questionary, *HAMD* Hamilton Depression Scale, *HIS* Hachinski Ischemic Score

[a] The *P* value was obtained by two-sample two-tailed *t* test

[b] The *P* value was obtained by two-tailed Pearson Chi square test

with memory complaints. All AD subjects underwent a complete physical and neurological examination, standard laboratory tests and neuropsychological assessments, which included mini-mental state examination (MMSE), World Health Organization-University of California-Los Angeles auditory verbal learning test (WHO-UCLA-AVLT), the Extended Scale for Dementia (ESD), montreal cognitive assessment (MoCA), clock drawing task (CDT), Activity of Daily Living Scale (ADL), Functional Activities Questionary (FAQ), Hamilton Depression Scale (HAMD) and Hachinski Ischemic Score (HIS). The diagnosis of AD fulfilled the new research criteria for possible or probable AD (Dubois et al. 2007, 2010). The patients were assessed with the clinical dementia rating (CDR) score (Morris 1993) as being in the early stages of AD (18 patients with CDR = 1 and 14 patients with CDR = 0.5). The HCs were recruited from the local community by advertisements. The inclusion criteria for HCs were as follows: (1) no neurological or psychiatric disorders, such as stroke, depression or epilepsy; (2) no neurological deficiencies, such as visual or hearing loss; (3) no abnormal findings, such as infarction or focal lesions in conventional brain magnetic resonance imaging (MRI); (4) no cognitive complaints; (5) MMSE score of 28 or higher; and (6) a CDR score of 0.

Data acquisition

MRI data acquisition was performed on a SIEMENS Trio 3-Tesla scanner (Siemens; Erlangen, Germany). Foam padding and headphones were used to limit head motion and reduce scanner noise. Functional images were collected axially using an echo-planar imaging (EPI) sequence with the following parameters: repetition time (TR)/echo time (TE)/flip angle (FA) = 2,000/40 ms/90°, field of view = 24×24 cm², resolution = 64×64 matrix, slices = 28, thickness = 4 mm, gap = 1 mm, voxel size = $3.75 \times 3.75 \times 4$ mm³ and bandwidth = 2,232 Hz/pixel. During the 478 s scan, subjects were instructed to hold still, keep their eyes closed and not to think of anything in particular. A simple questionnaire after the scan confirmed that none of subjects had fallen asleep. For registration purposes, high-resolution anatomical images were acquired using a 3D magnetization-prepared rapid gradient echo (MPRAGE) T1-weighted sequence with the following parameters: TR/TE/inversion time (TI)/FA = 1,900/2.2/900 ms/9°, resolution = 256×256 matrix, slices = 176, thickness = 1 mm, voxel size = $1 \times 1 \times 1$ mm³.

Data preprocessing

Data preprocessing were performed using the Statistical Parametric Mapping (SPM, www.fil.ion.ucl.ac.uk/spm) and data processing assistant for resting-state fMRI (DPARSF, www.restfmri.net/forum/DPARSF) (Yan and Zang 2010) toolkits. Briefly, preprocessing included removal of the first ten volumes, slice timing correction and head motion correction. To spatially normalize the fMRI data, the T1-weighted images were used to register the functional data to their corresponding anatomical image, and the resulting aligned T1 dataset was transformed into Montreal Neurological Institute (MNI) space (Ashburner and Friston 2005). To improve the coregistration of the fMRI data, a custom T1 template was built by averaging the normalized anatomical images across all subjects. Finally, the normalized functional images were created by applying the transformation of the T1 images to the customized T1 template. Notably, such a custom template-based registration procedure could reduce the inaccuracy of the spatial normalization of functional volumes due to GM atrophy in AD patients and healthy controls. Functional images were resampled to 3 mm isotropic voxels and spatially smoothed with a 4-mm full-width half-maximum (FWHM) Gaussian kernel. Linear detrending and temporal band-pass filtering (0.01–0.1 Hz) were applied to reduce the effect of low-frequency drifts and high-frequency physiological noise. Finally, several nuisance variables, including six head motion parameters, global mean signal, cerebrospinal fluid signal, and white matter signal were removed by multiple linear regression analysis. During image preprocessing, no subject was excluded due to excessive head motion (defined by a translation greater than 3 mm or rotation >3°), but five subjects (two AD and three HCs) were excluded due to failures in image normalization.

Definition of IPL subregions

We defined seven IPL subregions in each hemisphere using cytoarchitectonically defined probabilistic maps from the JuBrain Cytoarchitectonic Atlas (Zilles and Amunts 2010) as implemented in the SPM anatomy toolbox (Eickhoff et al. 2005) (www.fz-juelich.de/inm/inm-1/DE/Forschung/_docs/SPMAnatomyToolbox/SPMAnatomyToolbox_node.html). Voxels were included as potential IPL subregions only if the probability of their assignment to the IPL subregion was higher than any other nearby structure with a likelihood greater than 40 %. Each voxel was exclusively assigned to only one of the regions, which resulted in seven non-overlapping IPL subregions in each hemisphere, including the PF, PFcm, PFop, PFt and PFm of the SMG as regions of interest (ROIs) (Caspers et al. 2006, 2008) one through five and the PGa and PGp of the ANG as ROIs six and seven (Fig. 1). Each of the seven IPL subregions was shrunk by removing the voxels in its outer surface. This procedure can partly reduce the biasing effects of blood oxygen level-dependent (BOLD) signals on neighboring ROIs.
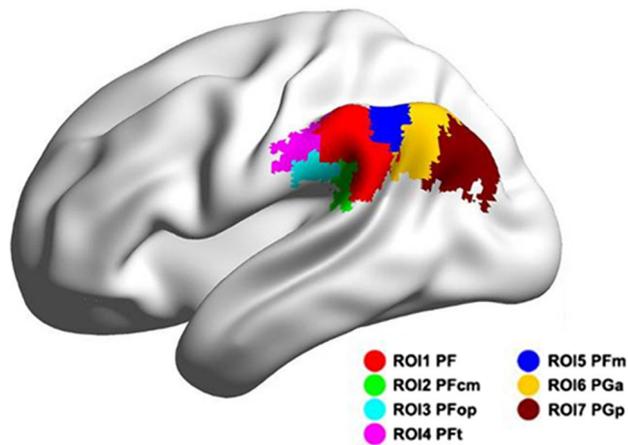
Fig. 1 The subregions of IPL. In each hemisphere, seven subregions were defined including supramarginal gyrus (PF, PFcm, PFop, PFt, PFm) and angular gyrus (PGa and PGp) using the anatomy toolbox in SPM8. *ROI* region of interest

RSFC analysis of the IPL subregions

The whole-brain intrinsic functional connectivity maps for each of the IPL subregions were computed as the Pearson correlation coefficient between the averaged time course of all of the voxels in the ROIs and every other voxel's time course within the GM mask. The GM mask was created by thresholding (a probability threshold of 0.2) the GM probability map obtained from all subjects in the present study. The resulting correlation coefficients were converted to z-scores using Fisher's r-to-z transformation to improve the normality. For each subject, we obtained 14 z-score maps that represented the intrinsic RSFC patterns of the 14 IPL subregions (seven for each hemisphere).

Hierarchical cluster analysis of the IPL subregional RSFCs

To determine whether these IPL subregions show similar or different RSFC patterns, we performed a hierarchal clustering analysis. To obtain the normal clustering pattern of the IPL subregions, this analysis was conducted only in the HC group. Briefly, for each IPL subregion, we performed one-sample t tests on the individual z-score maps to obtain a within-group statistical t map (see "Statistical analysis"), which was further converted to a z-map to normalize the RSFC strength distribution to a standard normal distribution. The z-maps represent the spatial RSFC characteristics of each IPL subregion across the healthy older adults. Subsequently, Pearson's correlation coefficients were computed between the pairs of standard z-maps, which resulted in a 14×14 correlation matrix. After converting the correlation matrix to a dissimilarity matrix (i.e., distance matrix by 1—correlation), which reflects the spatial

dissimilarity of every pair of the RSFC maps of the IPL subregions, we applied the average linkage agglomerative algorithm to the dissimilarity matrix to generate the agglomerative hierarchical cluster trees.

Statistical analysis

To examine the within-group RSFC patterns of each IPL subregion for the AD and HC groups, we performed one-sample t tests on individual z-score maps for each IPL subregion. The statistical significance threshold was set to $P < 0.01$ with a cluster size of 18 voxels (486 mm^3) based on Monte Carlo simulations (Ledberg et al. 1998) using the REST AlphaSim utility (www.restfmri.net, (Song et al. 2011), which corresponded to a corrected $P < 0.05$. Only clusters within the GM mask were retained.

To assess the between-group differences of the whole-brain RSFCs of each IPL subregion, we used general linear model (GLM) analysis (dependent variable: RSFCs; independent variable: group) with age and gender treated as covariates. The significance threshold was set to $P < 0.05$ with a cluster size of 42–52 voxels (the number of voxels varies for different IPL subregions), which corresponds to a corrected $P < 0.05$. The cluster size for each subregion was determined by Monte Carlo simulations, with the restriction that the significant clusters must belong to significant within-group connectivity maps for one or both groups. Considering the ambiguous biological interpretations of negative functional connections (Chai et al. 2012; Murphy et al. 2009; Fox et al. 2009; Weissenbacher et al. 2009), the statistical computations were limited in positive RSFCs.

To investigate the relationship between RSFC strength and cognitive behavior, we performed GLM analysis (dependent variable: RSFC; independent variable: MMSE score) for each IPL subregion with age and gender treated as covariates within the regions showing group differences. The statistical threshold was set to $P < 0.05$ with a cluster size of 9–18 voxels (the number of voxels varies for different IPL subregions), which corresponded to a corrected $P < 0.05$.

Validation analysis

Gray matter loss effect

As previous studies have demonstrated significant GM atrophy in AD patients (Busatto et al. 2003; Frisoni et al. 2002), the observed between-group differences in the RSFCs of the IPL subregions in our study might result from a structural abnormality in GM volume. To clarify this issue, we re-performed the GLM analysis to test the between-group differences in the RSFCs for each IPL subregion with GM volume as an additional covariate (Wang et al. 2011; He et al. 2007). Briefly, the GM volume

map of each individual was first estimated from the normalized T1 images using Voxel-Based Morphometry (VBM8 toolbox, http://dbm.neuro.uni-jena.de/vbm) (Ashburner and Friston 2000). Then, a two-sample t test between the AD group and HC group was performed to determine whether the GM was atrophied in AD patients. Finally, we reanalyzed the RSFC results by taking voxelwise GM volume as covariate.

Head motion effects

Recent R-fMRI studies have reported significant influences of head motion on RSFC analysis (Satterthwaite et al. 2012; Van Dijk et al. 2012; Power et al. 2012). To evaluate the effects of head motion on our results, two methods were employed in the validation analysis. First, we re-performed between-group statistical tests on the RSFC maps for each IPL subregion by regressing out the head motion measurements, which were calculated as the root mean squares (RMS) of the overall head displacement/rotation (Zuo et al. 2010). Second, we performed a 'scrubbing' procedure on the preprocessed images and re-performed the RSFC analysis and statistical tests (Power et al. 2012; Jenkinson et al. 2002). Briefly, we first calculated the framewise RMS deviation (dRMS) (Jenkinson et al. 2002) between the neighboring functional volumes within each subject and then scrubbed the volumes with a dRMS above 0.5 mm and their adjacent volumes (1 back and 2 forward) for each subject. This procedure partly reduced the bias on the R-fMRI signal induced by the head motion artifacts (Power et al. 2012).

Results

Demographic and neuropsychological tests

Demographic characteristics are shown in Table 1. No significant differences in gender or age were observed between the AD and HC groups (both $Ps > 0.01$). However, the AD group exhibited significantly lower MMSE, AVLT, ESD, MoCA, CDT, ADL and FAQ scores than the HC group ($Ps < 0.0001$).

Functional connectivity of the IPL subregions

Figure 2 illustrates the RSFC maps for each left IPL subregion within the HC and AD groups, which show similar patterns between the two groups by visual inspection. Morover, we used connectivity fingerprints to present the IPL connections to other cortical areas as Fig. 3. Given the similar functional connectivity patterns between left IPL and right IPL, we, therefore, put the RSFC results of right IPL subregions into supplementary materials (Figure S1). Here we focused on the

left IPL subregions. Based on the RSFC patterns in the HC group, we further used hierarchical clustering analysis to classify the seven IPL subregions into three zones along an anterior-to-posterior gradient (Fig. 4): the anterior zone along the regions of the PF, PFcm, PFop and PFt (ROI 1–4); the central zone of the PFm (ROI 5) and the posterior zone along the regions of the PGa and PGp (ROI 6 and 7). Thus, further description of the detailed RSFC patterns of the IPL subregions will be in terms of their different zones.

Within-group RSFCs of the IPL subregions

The anterior zone of the IPL (PF, PFcm, PFop and PFt; ROI 1–4) showed positive connectivity with the SMN regions, including the bilateral precentral gyrus (PreCG), postcentral gyrus (PoCG) and supplementary motor area (SMA), and the SN regions, including the dorsal anterior cingulate cortex (dACC), insula (INS), dorsal lateral prefrontal cortex (dlPFC), IPL, superior temporal gyrus (STG) and middle temporal gyrus (MTG). In addition, negative connectivity was observed with the DMN regions, including the medial prefrontal cortex (MPFC), precuneus (PCu)/ posterior cingulate cortex (PCC), ANG, lateral temporal cortex and medial temporal lobe.

The medial zone of the IPL (PFm, ROI 5) exhibited positive connectivity with the ECN regions, including the bilateral dorsal lateral and medial frontal cortex, IPL and MTG as well as a small cluster in the PCC. Negative connectivity was found mainly in the MPFC, anterior lateral temporal cortex, medial temporal lobe and occipital cortex.

The posterior zone of the IPL, such as the angular gyrus (PGa and PGp; ROI 6 and 7), was typically identified as a component of the DMN. Positive connectivity was found with the MPFC, PCu/PCC, dlPFC, lateral temporal and parietal cortices, which constituted the classical pattern of the DMN. Notably, we observed that the PGp (ROI 7) had significant positive RSFC with the medial temporal lobe and that the PGa (ROI 6) showed significant negative RSFC to these regions. We found other negative connectivity of these two subregions in the sensorimotor cortex, visual cortex and INS.

Between-group differences in the RSFCs of the IPL subregions

The last column of Fig. 2 illustrates the between-group differences of the RSFC for each IPL subregion. In this study, we only focused on the positive RSFC because the negative RSFC remains controversial. Some researchers hold the idea that a negative RSFC is an artifact of global signal regression (Murphy et al. 2009); however, others take it as anti-correlated functional networks (Hampson et al. 2010).

Fig. 2 Resting-state functional connectivity within group and between maps of left IPL subregions. *First column* shows the subregions defined in IPL. The *second* and *third columns* show the within-group statistical maps of HCs and patients with AD, respectively, with statistical threshold set at $P < 0.05$, corrected. *Hot* and *cold colors* represent positive and negative functional connections, respectively. *Last column* shows the between-group statistical maps, with statistical threshold set at $P < 0.05$, corrected. *Hot* and *cold colors* represent increased and decreased functional connectivities in Alzheimer's disease group compared with healthy control group, respectively. The results were mapped on cortical surface using the BrainNet Viewer (www.nitrc.org/projects/bnv/) (Xia et al. 2013). *ROIs* regions of interest, *NC* normal control, *AD* Alzheimer's disease
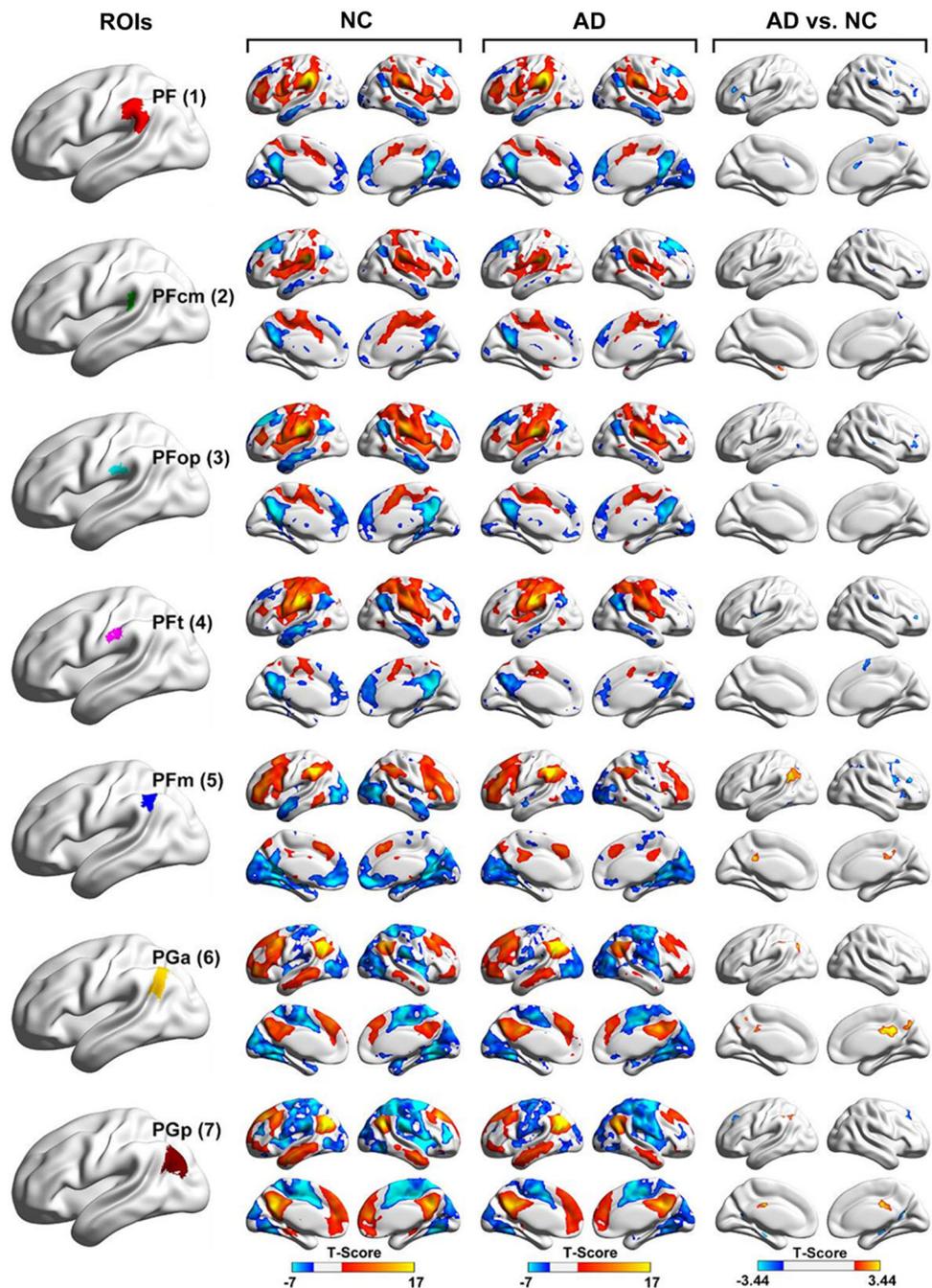
When comparing the RSFCs of the anterior zone of the IPL (PF, PFcm, PFop and PFt; ROIs 1–4) between the AD and HC groups, we found significantly decreased RSFCs in AD patients in regions mainly located within the SMN and SN. The detailed regions were as follows: for the PF (ROI 1), we observed decreased RSFC mainly in the SMN region of the right PoCG and SN regions of the bilateral INS, dlPFC, right dACC, IPL and STG. For the PFcm (ROI 2), the differential regions included the SMN region of the right PoCG and SN regions of the

right dlPFC and STG. For the PFop (ROI 3), we observed decreased RSFC in the SMN region of the right PoCG as well as the SN regions of the bilateral INS, dlPFC, IPL, right STG and MTG. For the PFt (ROI 4), the regions with significantly decreased RSFCs included the SMN regions of the right PoCG and left PreCG as well as the SN region of the right dlPFC. In addition, we observed significantly increased RSFCs of the PFcm (ROI 2) to the right putamen and left STG in the AD group (see Fig. 5; Table 2).
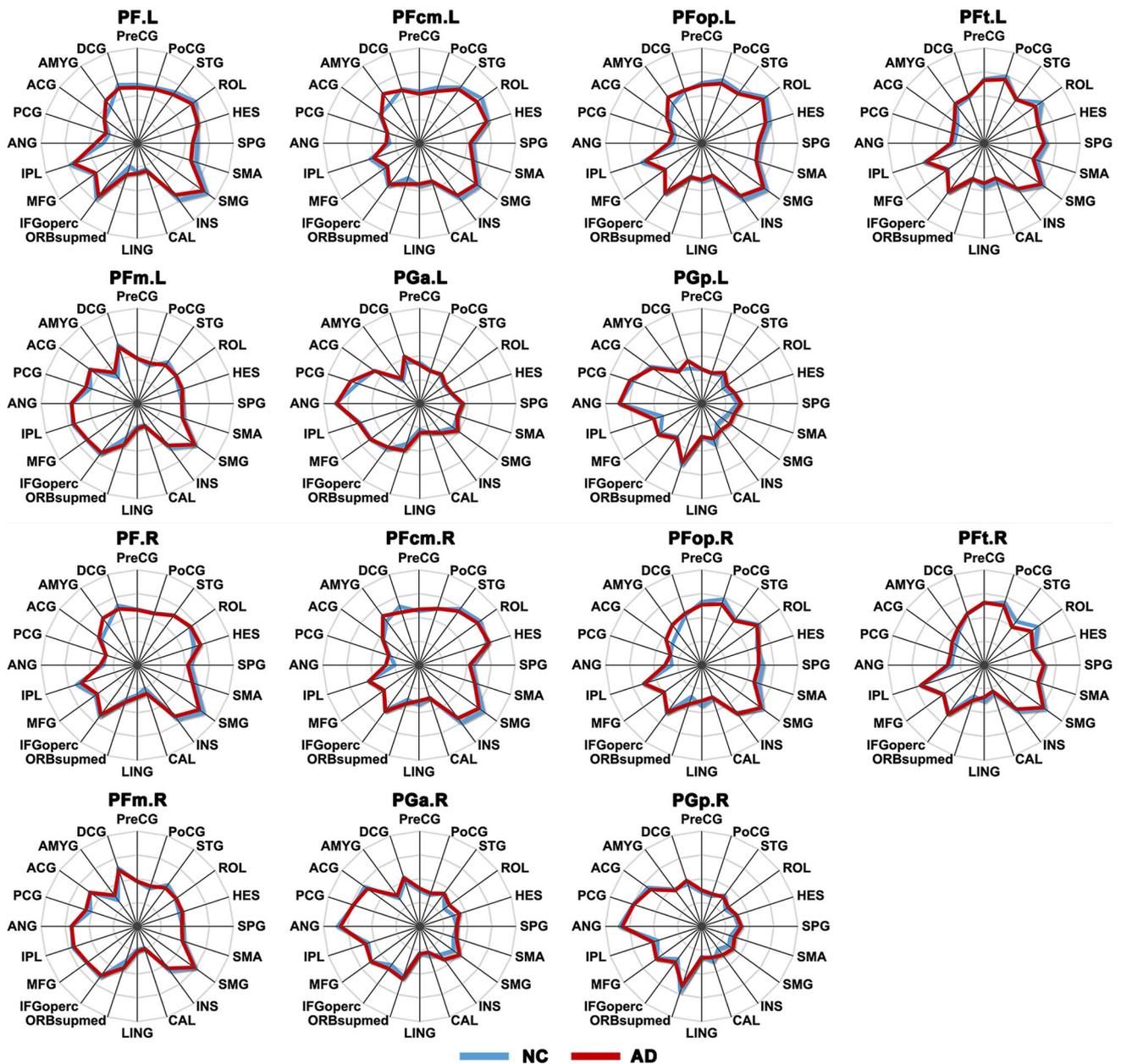
Fig. 3 RSFC fingerprints of the IPL subregions. The fingerprints depict the mean RSFC between each IPL subregion and several key regions in both AD and HC groups. Visual examination indicated that there was a similar RSFC fingerprint among the PF, PFcm, PFop and PFt, and between the PGa and PGp. Similar RSFC fingerprints can be found in the right IPL subregions. *L* left, *R* right, *PreCG* precentral gyrus, *PoCG* postcentral gyrus, *STG* superior temporal gyrus, *ROL* rolandic operculum, *HES* heschl gyrus, *SPG* superior parietal gyrus, *SMA* supplementary motor area, *SMG* supramarginal gyrus, *INS* insula, *CAL* calcarine cortex, *LING* lingual gyrus, *ORBsupmed* superior frontal gyrus (medial orbital), *IFGoperc* inferior frontal gyrus (opercular part), *MFG* middle frontal gyrus, *IPL* inferior parietal lobule, *ANG* angular gyrus, *PCG* posterior cingulate gyrus, *ACG* anterior cingulate and paracingulate gyri, *AMYG* amygdala, *DCG* median cingulate and paracingulate gyri

Compared with the HCs, the AD patients showed decreased RSFCs with the PFm (ROI 5) in the ECN regions, including the right middle frontal gyrus (MFG), inferior frontal gyrus (IFG) and IPL as well as the left MTG. Moreover, increased RSFCs with the PFm (ROI 5) in the AD group were found in the left IPL and right PCC (see Fig. 5; Table 3).

In the AD group, PGp (ROI 7) showed significantly decreased connectivity with the DMN regions, including the bilateral dlPFC, the bilateral medial
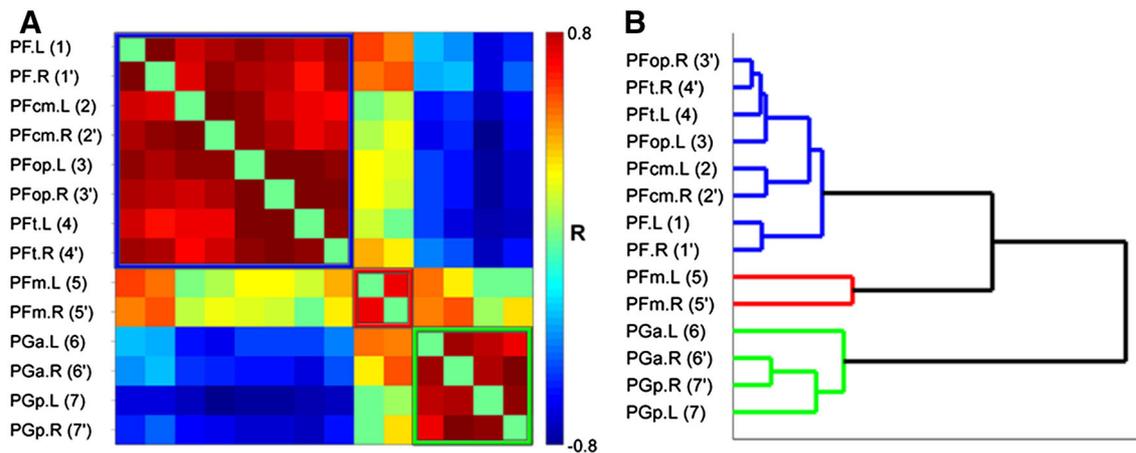
Fig. 4 Spatial hierarchy clustering of IPL subregions in HCs. **a** The correlation matrix was estimated by calculating the Pearson's correlation coefficients each pairs of the within group statistical maps of subregions. **b** Hierarchy clustering using correlation distance revealed three clusters from the 14 subregions in two hemispheres: the part of PF (1), PFcm (2), PFop (3) and PFt (4) colored in *blue*; the part of PFm (5) colored in *red*; and PGa (6) and PGp (7) colored in *green*. The *numbers* in the *brackets* refer to the region of interest. The apostrophe refers to subregions in right hemisphere. *ROI* region of interest
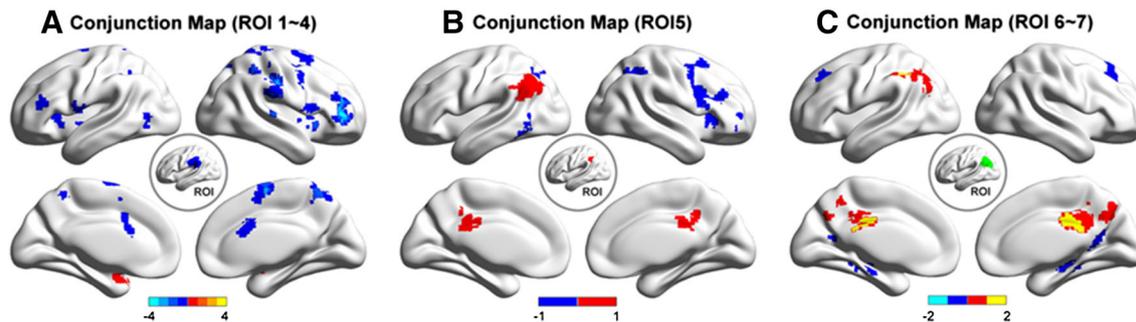
Fig. 5 The conjunction maps of between-group differences from three kinds of IPLsubregions. RSFC between-group differences of RSFC of **a** the anterior IPL (PF, PFcm, PFop and PFt; ROI 1–4); **b** the central IPL (PFm; ROI 5); and **c** the posterior IPL (PGa and PGp; ROI 6 and 7). *Colorbar* indicates the frequency that the region emerged in between group comparisons. *Hot* and *cold colors* represent increased and decreased functional connectivities in Alzheimer's disease group compared with healthy control group, respectively. *ROI* region of interest

temporal lobe and right PCC. In addition, the increased RSFC to the PGa (ROI 6) and PGp (ROI 7) was found in the left IPL and PCu/PCC in the AD (see Fig. 5; Table 4).

Relationship between the RSFCs of the IPL subregions and cognitive behavior

In the AD group, we found positive correlations between the MMSE scores and the IPL subregional RSFCs, including connectivity between the left PF (ROI 1) and right SMG, the left PFcm (ROI 2) and right STG, the left PFm (ROI 5) and right MFG as well as the left PFm (ROI 5) and right IFG. We also found a negative correlation between the MMSE scores and connectivity between left PFop (ROI 3) and right MTG (Fig. 6). Besides, we also found significant correlations between cognitive behavior

scores (i.e., AVLT, ESD, MoCA, CDT and ADL) and the IPL subregional RSFCs (see Table 5 for detail).

The reproducibility of our results

Gray matter loss effect

AD patients showed significant and widespread reduction in GM volume compared with the HCs. The most atrophied regions included the lateral temporal cortex, medial temporal lobe, dorsal and medial frontal cortices, dACC, PCu/PCC, INS as well as the subcortical regions of the IPL (Fig. 7). After the gray matter correction, most detected regions remained significant, although their cluster size was smaller compared to the analysis without the GM correction (Fig. 7). For the PF, PFcm, PFop and PFt (ROI 1–4), some regions that showed AD-related decreases in

Table 2 Regions showing AD-related RSFC changes in IPL sub-regions (ROI 1–4)

ROIs	Brain regions	BA	Cluster voxels	MNI coordinates (mm)			Maximum Z
				x	y	z	
PF.L (1)	L. IFG/INS	47/13	139	−39	33	15	−4.26
	L. Cerebellum	NA	67	−30	−45	−54	−4.19
	R. IFG	44	79	57	12	9	−4.00
	R. PoCG/IPL	40	325	66	−27	18	−3.83
	R. ACC	24	97	0	18	24	−3.39
	R. MFG	6	102	33	−3	54	−3.35
	R. INS/IFG	13/47	90	39	18	−3	−3.34
	R. SFG	6	137	24	0	69	−3.30
	R. PCu	7	59	6	−54	60	−3.13
	R. MFG	10	117	36	42	0	−2.92
PFcm.L (2)	L. PCu	7	54	−15	−45	57	−3.62
	R. STG	42	50	63	−24	6	−3.37
	R. PoCG	7	150	9	−36	66	−2.94
	R. MFG/IFG	10	54	39	51	3	−2.81
	R. Putamen	NA	57	21	3	−9	3.52
	L. STG	38	47	−30	6	−24	2.95
PFop.L (3)	R. MTG	37/19	61	−54	−75	0	−3.79
	R. IFG/MFG	10/46	140	45	42	9	−3.64
	R. INS	13	70	45	9	−3	−3.46
	L. INS/IFG	13/46	48	−33	21	12	−3.46
	R. IPL	40	56	30	−42	51	−3.31
	R. STG/PoCG	42/43	74	60	−24	9	−3.21
	L. INS	13	80	−27	−18	−6	−3.15
	L. SFG	6	67	−12	−6	72	−3.08
	R. PoCG	4	60	63	−18	42	−2.83
	L. IPL	40	68	−33	−51	39	−2.72
PFt.L (4)	L. PreCG	4	129	−57	−6	12	−3.79
	R. PoCG	2	84	63	−24	45	−3.58
	R. IFG	46	47	45	45	6	−3.42
	R. SFG/MFG	6	109	9	0	69	−3.10

Between-groups differences were determined by two-sample t tests ($P < 0.05$, corrected)

ROIs regions of interest, *BA* Brodmann's area, *MNI* Montreal Neurological Institute, *x, y, z* coordinates of primary peak locations in the MNI space, *Z* statistical value of peak voxel showing differences between two groups, *NA* not applicable, *L* left, *R* right, *IFG* inferior frontal gyrus, *INS* insula, *PoCG* postcentral gyrus, *IPL* inferior parietal lobule, *ACC* anterior cingulate gyrus, *MFG* middle frontal gyrus, *SFG* superior frontal gyrus, *PCu* precuneus, *STG* superior temporal gyrus, *MTG* middle temporal gyrus, *PreCG* precentral gyrus

RSFCs were no longer significant after the GM correction, including the bilateral INS, ACC, right dorsal frontal cortex, sensorimotor cortex, SMG and left PCu. For the PFm (ROI 5), an additional region of left dorsal superior frontal gyrus (SFG) showed increased connectivity in AD patients after the GM correction. For the PGa and PGp (ROI 6 and 7), previously significant regions in the bilateral dorsal frontal and medial temporal cortices were eliminated, whereas a new set of regions located in the lateral and medial prefrontal cortices showed decreased RSFC, and the right IPL showed increased RSFC after GM correction.

Head motion effects

We evaluated the effects of head motions in two ways, regressing covariance and 'scrubbing'. (1) There was no significant head motion differences between the AD and HC groups in either displacement ($T = 0.98$, $P = 0.33$) or rotation ($T = 1.63$, $P = 0.11$). After using the head displacement/rotation as the extra covariate, we reanalyzed our data and found the same effects as in our uncorrected analysis. (2) After performing the 'scrubbing' procedure in the preprocessed images, we discarded a mean number of 3.13 % (range 0–43.23 %, 56 of the 70 individuals were scrubbed less than five frames) of images across all subjects. For details, 2.88 %, 0–25.33 %, 25 of the 32 individuals were scrubbed less than five frames in AD; 3.34 %, 0–43.23 %, 31 of the 38 individuals were scrubbed less than five frames in HCs. Further statistical analysis revealed that almost all of the previous results remained significant.

Table 3 Regions showing AD-related RSFC changes in IPL sub-region (ROI 5)

ROI	Brain regions	BA	Cluster voxels	MNI coordinates (mm)			Maximum Z
				x	y	z	
PFm.L (5)	R. MFG	6	584	27	3	51	−4.36
	L. MTG	37	92	−42	−57	3	−3.81
	L. IPL	7	103	−30	−72	27	−3.78
	R. IFG	47	49	36	21	−3	−3.47
	R. IPL	40	221	33	−57	33	−3.31
	L. Cerebellum	NA	58	−18	−69	−45	−3.09
	L. SMG	39	267	−54	−57	27	4.20
	R. PCC	31	213	0	−42	30	3.95

Between groups differences were determined by two-sample *t* tests (*P* < 0.05, corrected)

ROI region of interest, *BA* Brodmann's area, *MNI* Montreal Neurological Institute, *x, y, z* coordinates of primary peak locations in the MNI space, *Z* statistical value of peak voxel showing differences between two groups, *NA* not applicable, *L* left, *R* right, *MFG* middle frontal gyrus, *MTG* middle temporal gyrus, *IFG* inferior frontal gyrus, *IPL* inferior parietal lobule, *SMG* supramarginal gyrus, *PCC* posterior cingulate cortex

Table 4 Regions showing AD-related RSFC changes in IPL sub-regions (ROI 6–7)

ROIs	Brain regions	BA	Cluster voxels	MNI coordinates (mm)			Maximum Z
				x	y	z	
PGa.L (6)	R. PCC	31	415	3	−42	36	4.86
	R. Cerebellum	NA	57	54	−57	−30	3.83
	L. ANG/IPL	39	93	−48	−72	39	3.47
	L. Precuneus	7	105	−6	−66	36	3.43
	L. IPL	40	68	−57	−42	48	3.08
PGp.L (7)	L. PHG	36	65	−27	−21	−18	−4.47
	R. PCC	30	167	15	−57	15	−3.57
	L. MFG/SFG	8/9	84	−24	33	42	−3.57
	R. PHG	36	81	39	−30	−15	−3.60
	R. SFG	8	77	18	30	54	−3.27
	L. Cerebellum	NA	62	−21	−90	−30	−3.18
	L. IPL	40	247	−57	−42	48	4.02
	L. PCC	23	130	−6	−21	30	3.77

Between groups differences were determined by two-sample *t* tests (*P* < 0.05, corrected)

ROIs regions of interest, *BA* Brodmann's area, *MNI* Montreal Neurological Institute, *x, y, z* coordinates of primary peak locations in the MNI space, *Z* statistical value of peak voxel showing differences between two groups, *NA* not applicable, *L* left, *R* right, *ANG* angular gyrus, *IPL* inferior parietal lobule, *PHG* parahippocampal gyrus, *PCC* posterior cingulate cortex, *MFG* middle frontal gyrus, *SFG* superior frontal gyrus

Discussion

By applying RSFC analysis to R-fMRI data acquired from HCs and AD patients, we observed three distinctive patterns of functional connectivity for the subregions of the IPL. These patterns defined an anterior-to-posterior functional subdivision of the IPL: (1) the anterior zone of the IPL exhibited functional connectivity with the SMN and SN regions; (2) the central zone of the IPL functionally connected with the ECN regions; and (3) the posterior zone of the IPL was involved in the DMN regions. Importantly,

the AD patients showed differentially disrupted patterns of RSFCs in the subregions within different functional networks (SMN, SN, ECN and DMN), which were significantly associated with cognitive impairment.

Functional connectivity of the IPL subregions

The anterior zone of the IPL (ROIs 1–4) was functionally connected to several SMN regions (PreCG, PoCG and SMA) and SN regions (dACC, INS, dlPFC, IPL, STG and MTG). Tracing studies in macaques have revealed that the
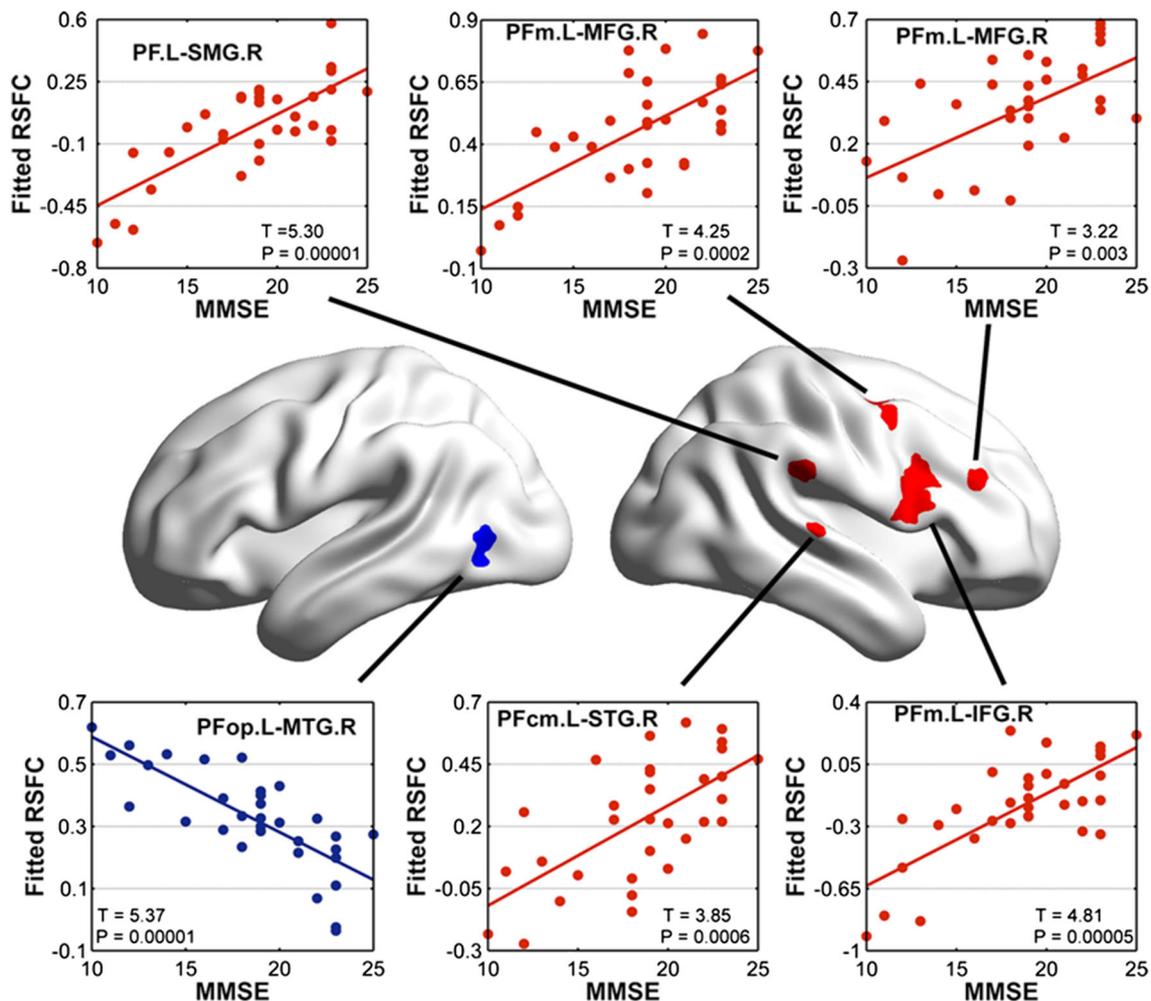
Fig. 6 Correlation of clinical variables and resting-state functional connectivity of IPL subregions. *RSFC* resting-state functional connectivity, *MMSE* mini-mental state examination, *ROI* region of interest, *SMG* supramarginal gyrus, *MFG* middle frontal gyrus, *MOG* middle occipital gyrus, *MTG* middle temporal gyrus, *IFG* inferior frontal gyrus, *L* left, *R* right

anterior IPL shows strong anatomical connections with the sensorimotor cortex (Cavada and Goldman-Rakic 1989a, b; Gregoriou et al. 2006). Using diffusion MRI (dMRI) and probabilistic tractography in humans, researchers found that the anterior IPL predominantly follows the tracts of the superior longitudinal fascicle (SLF) and arcuate fascicle (AF) the sensorimotor cortex (Makris et al. 2005; Caspers et al. 2011). Functionally, several task-based fMRI studies have demonstrated that the anterior IPL is involved in sensorimotor processing, such as object manipulation (Binkofski et al. 1999), tool use (Peeters et al. 2009), motor execution and imagery (Hanakawa et al. 2008). Furthermore, researchers also observed the RSFC between the anterior IPL and sensorimotor cortex in several recent R-fMRI studies (Mars et al. 2011; Wang et al. 2012a). These findings, along with our results, suggest that the anterior IPL plays an important role in the SMN. In addition, we found that the anterior IPL functionally connected

to the SN regions. In macaques, the anterior IPL show anatomically connection with the inferior frontal and posterior temporal regions (Cavada and Goldman-Rakic 1989a, b; Gregoriou et al. 2006). Similarly, dMRI in humans has revealed anatomical connections of the anterior IPL to the inferior frontal cortex and INS (Caspers et al. 2011). Furthermore, fMRI studies have found that the anterior IPL (SMG) along with the ACC, INS, dorsal frontal cortex, STG and ITG constitutes the salience network (Downar et al. 2002), which is sensitive to stimulus salience (Seeley et al. 2007; Uddin et al. 2011). Collectively, our findings suggest that the anterior zone of the IPL is involved in the functional integration of the SMN and SN.

The central zone of the IPL (ROI 5) is functionally connected to the core ECN regions, including the dorsal lateral and medial frontal cortex, IPL and MTG. Using dMRI and tractography approaches, researchers have found that the central IPL shows consistent fiber tracts (SLF and

Table 5 Regions showing correlation between cognitive behaviors and IPL sub-regional connectivities in the AD patients

Cognitive score	ROIs	Brain regions	BA	Cluster voxels	MNI coordinates (mm)			Maximum T
					x	y	z	
MMSE	PF.L (1)	R. IFG	44	28	54	6	15	3.37
		R. SMG	40	54	60	−30	21	5.30
		R. MFG	6	42	33	0	57	3.86
	PFcm.L (2)	R. STG	42	16	60	−21	9	3.85
	PFop.L (3)	L. MOG	37	35	−45	−63	−3	−5.37
	PFm.L (5)	R. IFG	44	92	51	15	21	4.81
		R. MFG	46	26	39	36	27	3.22
		R. MFG	6	34	45	6	51	4.25
		R. MFG	6	20	30	3	57	2.65
AVLT	PF.L (1)	R. PreCG	44	19	63	6	9	2.95
		R. SMG	40	16	60	−30	21	3.19
	PFcm.L (2)	R. STG	42	13	63	−27	9	3.15
		R. SMG	40	9	69	−9	15	3.57
	PFop.L (3)	L. MOG	37	16	−45	−66	−3	−4.02
		R. PoCG	3	17	30	−36	48	−4.65
ESD	PGa.L (6)	L. IPL	40	18	−51	−48	51	4.07
MoCA	PF.L (1)	L. Cerebellum	NA	31	−39	−42	−42	3.90
		R. SMG	40	45	60	−30	18	3.91
		R. MFG	6	42	30	−3	48	4.55
	PFop.L (3)	L. MOG	37	25	−45	−63	−3	−3.99
	PFm.L (5)	R. IFG	9	75	51	15	21	3.67
		R. MFG	46	19	39	36	27	3.16
		R. PreCG	6	20	30	0	45	2.72
CDT	PF.L (1)	L. Cerebellum	NA	31	−30	−42	−45	4.47
		R. MFG	6	39	33	0	57	5.12
		R. PoCG	2	25	48	−39	57	3.89
	PFcm.L (2)	R. AMYG	NA	11	24	0	−9	−2.91
	PFop.L (3)	L. IOG	37	22	−45	−63	−3	−3.43
	PFm.L (5)	R. IFG	9	42	51	12	18	3.78
		R. MFG	6	43	27	0	51	2.98
	PGp.L (7)	R. PHG	36	24	33	−33	−15	−3.29
		L. CAL	17	15	−6	−63	15	−3.24
		R. CAL	17	25	6	−63	18	−3.33
ADL	PF.L (1)	L. Cerebellum	NA	33	−33	−42	−45	−4.80
		R. IFG	44	15	57	18	9	−2.82
		R. SMG	40	40	57	−27	30	−3.52
		R. PreCG	6	19	54	9	39	−3.07
	PFm.L (5)	B. DCG	31	20	0	−33	42	3.35
	PGa.L (6)	L. IPL	40	18	−54	−42	42	2.91
	PGp.L (7)	L. Cerebellum	NA	19	−21	−87	−39	−3.62
		R. PCu	31	23	12	−54	15	−3.31
		L. IPL	40	17	−48	−57	48	3.14

Correlations between cognitive score and functional connectivities were determined by GLM ($P < 0.05$, corrected)

ROIs regions of interest, *BA* Brodmann's area, *MNI* Montreal Neurological Institute, *x*, *y*, *z* coordinates of primary peak locations in the MNI space, *T* statistical value of peak voxel showing significant correlation, *NA* not applicable, *L*, left, *R* right, *B* bilateral, *MMSE* mini-mental state examination, *AVLT* auditory verbal learning test, *ESD* The Extended Scale for Dementia, *MoCA* montreal cognitive assessment, *CDT* clock drawing task, *ADL* Activity of Daily Living Scale, *IFG* inferior frontal gyrus, *SMG* supramarginal gyrus, *MFG* middle frontal gyrus, *STG* superior temporal gyrus, *MOG* middle occipital gyrus, *PreCG* precentral gyrus, *PoCG* postcentral gyrus, *IPL* inferior parietal lobule, *AMYG* amygdala, *IOG* inferior occipital gyrus, *PHG* parahippocampal gyrus, *CAL* calcarine sulcus, *DCG* middle cingulate gyrus, *PCu* precuneus

AF) to the dorsal frontal regions, lateral parietal regions and temporal regions (Caspers et al. 2011). Furthermore, this subregion is involved in several cognitive control and executive tasks (Crone et al. 2006) and is also identified as a functional component of the frontoparietal control system in R-fMRI studies (Dosenbach et al. 2007; Vincent et al. 2008). Our results are largely compatible with these previous studies.
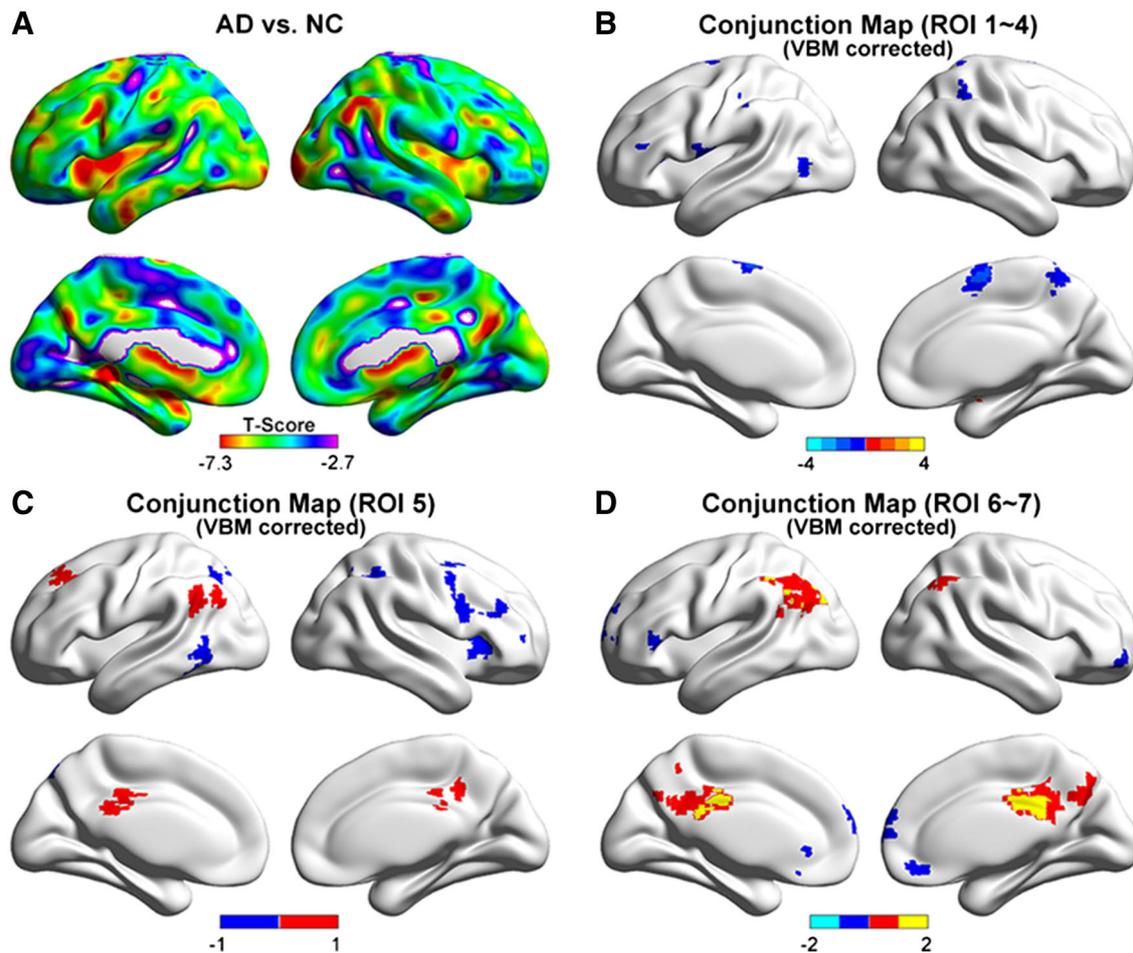
Fig. 7 The effects of GM volume loss. **a** The between-group differences of GM volume with a threshold of $P < 0.05$, FDR corrected. The GM volume was corrected during the between-group comparisons in RSFC by adding it as an additional covariate in the GLM analysis. Conjunction maps of between-group differences in RSFC of **b** the anterior IPL (PF, PFcm, PFop and PFt; ROI 1–4); **c** the central IPL (PFm; ROI 5); and **d** the posterior IPL (PGa and PGp; ROI 6 and 7) after GM volume correction

We noticed that the posterior zone of the IPL (ROIs 6–7) exhibited functional connectivity with several DMN regions. Tracing studies in macaques found that the posterior IPL exhibited anatomical connections mainly to the limbic regions, such as the PCC and parahippocampal gyrus (Cavada and Goldman-Rakic 1989a, b). In human dMRI studies, the posterior IPL mainly follow tracts of the inferior longitudinal fascicle (ILF) and the extreme capsule to reach the entire temporal lobe and the orbitofrontal cortex (Caspers et al. 2011; Rushworth et al. 2006). Moreover, many R-fMRI studies have observed that the IPL is functionally connected to the MPFC, PCu/PCC and medial temporal lobe, which are the well-known components of the DMN (Buckner et al. 2008).

Disrupted IPL subregion functional connectivity in AD

We found that the subregions of the IPL showed differentially disrupted functional connectivity patterns in AD.

Specifically, we observed disrupted connectivities between the anterior zone (ROIs 1–4) and the SMN and SN regions, between the central zone (ROI 5) and ECN regions, as well as between the posterior zone (ROIs 6–7) and DMN regions.

The anterior zone of the IPL exhibited decreased connectivity with several SMN regions in AD patients. Task-related fMRI studies have reported decreased activation in the SMA and premotor cortex in AD during performance of motor-related tasks (Agosta et al. 2010; Vidoni et al. 2012). Based on a large cohort of 510 human subjects, a recent R-fMRI study found that the SMN was preferentially affected in AD patients (Brier et al. 2012). Combined with these findings, we speculate that along with subtle motor impairment in AD, the functions of the sensorimotor system might be impaired. We also observed decreased connectivity between the anterior IPL and several SN regions in the AD patients. Previous structural MRI studies have demonstrated AD-related GM loss in the INS,

cingulate gyrus and IPL (Guo et al. 2010). Furthermore, R-fMRI studies revealed reduced RSFC of the SN in mild AD (Brier et al. 2012). These findings are consistent with those of previous studies. In addition, the regions of the putamen and STG showed increased connectivity to the PFcm (ROI 2). Using arterial spin-labeling perfusion, a recent MRI study found increased regional cerebral blood flow (CBF) in the putamen in early AD patients (Dai et al. 2009). In addition, increased functional connectivity between the parietal and temporal regions has been found in the early-stage of AD (Jacobs et al. 2012). The increases in the CBF and functional connectivity, in addition to our findings, suggest that AD patients could utilize additional different brain areas and employ unique strategies for storing and recalling information, presumably as a compensatory mechanism for cognitive decline (Becker et al. 1996; Grady et al. 2003).

The central zone of the IPL in AD patients exhibited decreased connectivity with the ECN regions, including the right MFG, IFG, IPL and left MTG. Task-related studies have revealed that AD patients have reduced PET activation in the right frontal cortex and MTG (Johannsen et al. 1999) and reduced fMRI activation in the left frontal and parietal regions (Hao et al. 2005). R-fMRI studies have also found disrupted functional connectivity within the ECN regions in AD patients (Agosta et al. 2012; Brier et al. 2012) and in individuals at high risk for AD (Liang et al. 2011). Here, we have provided further evidence for AD-related disruption of the ECN. Notably, two parietal regions of the left SMG and bilateral PCC showed increased connectivity in AD patients. Increased connectivity within the parietal lobe has been found in AD during a visuospatial task (Jacobs et al. 2012). Furthermore, an R-fMRI study found that AD patients exhibited increased connectivity in the right SMG (Agosta et al. 2012). Our study, the increased connectivity of the SMG and PCC to the PFm are in line with previous studies, which suggested compensatory neural activity in AD patients.

Decreased functional connectivity to the posterior zone of the IPL was involved in the DMN regions in AD patients, including the medial temporal lobe, dlPFC and PCC. Many neuroimaging studies have demonstrated the structural and functional abnormalities of DMN regions in AD, such as cortical thinning (Dickerson and Sperling 2009), amyloid deposition (Buckner et al. 2009), decreased intrinsic brain activity (He et al. 2007; Wang et al. 2011) and disrupted functional connectivity of these regions (Greicius et al. 2004). Our findings provide further evidence for the disconnection of the DMN in AD, which is especially relevant to the posterior part of the IPL. We also observed that IPL and PCC/PCu showed increased connectivity to the posterior IPL in AD patients. A previous fMRI study demonstrated AD-related over-activation in the

parietal region during a face-name recognition task (Pariente et al. 2005). Another fMRI study revealed increased activation of the PCC in people with high AD risk factors during a semantic memory task, which suggests the functional recruitment of this region (Seidenberg et al. 2009). Thus, we speculate that the increased connectivity in the IPL and PCC/PCu might imply compensation for a disconnection of the DMN in AD.

Comparison with IPL receptor architecture analysis

Our study showed that different subregions of the IPL had differential RSFC patterns, which are well in line with the findings of receptor architectonics in IPL (Caspers et al. 2013). Notably, Caspers et al. (2013) investigated the distribution of 15 different receptors from 6 classical neurotransmitter systems including glutamatergic, γ-aminobutyric acid-ergic, cholinergic, adrenergic, serotoninergic and dopaminergic receptors. Using hierarchical clustering analysis of the receptor distribution, they classified the human IPL into rostral, middle and caudal groups, which correspond to the well-known cytoarchitectonic, connectional and functional diversity at the molecular level. Further comparison of receptor distribution with other cortical areas showed high similarities with Broca's region for all three groups, with the superior parietal cortex for the middle group and with extrastriate visual areas for the caudal group.

Interestingly, numerous evidences have implicated the effects in these receptors in the pathological mechanisms of AD (Barrantes et al. 2010; Medeiros et al. 2011; Xu et al. 2012). The modification of these receptors may be associated with amyloid plaque formation and tau neurotoxicity and mediate the subsequent oxidative stress related to neuronal toxicity, which finally results in cognitive impairment (Xiong et al. 2004). In these previous studies, AD patients showed significant reductions in glutamate receptor (Hanyu et al. 2012; Mishizen-Eberz et al. 2004; Proctor et al. 2011), γ-aminobutyric acid receptors (Limon et al. 2012), nicotinic acetylcholine receptors (Sabbagh et al. 2006), adrenergic receptors (Laureys et al. 2010), serotoninergic receptors (Lai et al. 2005; Truchot et al. 2008) and dopaminergic receptors (Kemppainen et al. 2000). On the basis of these studies, we speculated that our findings of differentially impaired functional connectivity patterns in IPL subregions in AD might reflect different receptor defects at the molecular level.

Future considerations

Several issues need further consideration. First, in the current study, we mainly focused on the R-fMRI functional connectivity of the IPL sub-regions. Further studies that simultaneously combine the R-fMRI and dMRI data would

reveal structural substrates underlying these functional deficits in AD. Second, recent studies have paid more attention to individuals at high risk for AD, such as amnestic mild cognitive impairments (Wang et al. 2013; Bai et al. 2012) and ApoE-4 allele carriers (Pievani et al. 2011b). Exploring these populations would provide valuable biomarkers for the early diagnosis of AD. Finally, a longitudinal design would be crucial to elucidate the progressive changes in the IPL sub-regional connectivity. Such an approach may provide predictive insight into understanding the pathophysiological mechanism of AD.

Conclusion

We have identified abnormal functional connectivity of IPL sub-regions in AD patients and have observed the patterns of abnormalities varies in different IPL sub-regions, which involved in different functional brain networks such as SMN, SN, ECN and DMN. These findings have important implications for the underlying neurobiology of AD and add the new evidence for the disconnection syndrome of AD, which may provide the potential biomarker for detecting early AD in the future.

Conflict of interest The authors declare no competing financial interests.

References

Agosta F, Rocca MA, Pagani E, Absinta M, Magnani G, Marcone A, Falautano M, Comi G, Gorno-Tempini ML, Filippi M (2010) Sensorimotor network rewiring in mild cognitive impairment and Alzheimer's disease. Hum Brain Mapp 31(4):515–525

Agosta F, Pievani M, Geroldi C, Copetti M, Frisoni GB, Filippi M (2012) Resting state fMRI in Alzheimer's disease: beyond the default mode network. Neurobiol Aging 33(8):1564–1578

Allen G, Barnard H, McColl R, Hester AL, Fields JA, Weiner MF, Ringe WK, Lipton AM, Brooker M, McDonald E, Rubin CD, Cullum CM (2007) Reduced hippocampal functional connectivity in Alzheimer disease. Arch Neurol 64(10):1482–1487

Ashburner J, Friston KJ (2000) Voxel-based morphometry—the methods. Neuroimage 11(6 Pt 1):805–821

Ashburner J, Friston KJ (2005) Unified segmentation. NeuroImage 26(3):839–851

Bai F, Shu N, Yuan Y, Shi Y, Yu H, Wu D, Wang J, Xia M, He Y, Zhang Z (2012) Topologically convergent and divergent structural connectivity patterns between patients with remitted geriatric depression and amnestic mild cognitive impairment. J Neurosci 32(12):4307–4318

Barrantes FJ, Borroni V, Valles S (2010) Neuronal nicotinic acetylcholine receptor-cholesterol crosstalk in Alzheimer's disease. FEBS Lett 584(9):1856–1863

Becker JT, Mintun MA, Aleva K, Wiseman MB, Nichols T, DeKosky ST (1996) Compensatory reallocation of brain resources supporting verbal episodic memory in Alzheimer's disease. Neurology 46(3):692–700

Binkofski F, Buccino G, Stephan KM, Rizzolatti G, Seitz RJ, Freund HJ (1999) A parieto-premotor network for object manipulation: evidence from neuroimaging. Exp Brain Res Experimentelle Hirnforschung 128(1–2):210–213

Biswal B, Yetkin FZ, Haughton VM, Hyde JS (1995) Functional connectivity in the motor cortex of resting human brain using echo-planar MRI. Magn Reson Med 34(4):537–541

Braak H, Braak E (1991) Neuropathological stageing of Alzheimer-related changes. Acta Neuropathol 82(4):239–259

Brier MR, Thomas JB, Snyder AZ, Benzinger TL, Zhang D, Raichle ME, Holtzman DM, Morris JC, Ances BM (2012) Loss of intranetwork and internetwork resting state functional connections with Alzheimer's disease progression. J Neurosci 32(26):8890–8899

Buckner RL, Andrews-Hanna JR, Schacter DL (2008) The brain's default network: anatomy, function, and relevance to disease. Ann N Y Acad Sci 1124:1–38

Buckner RL, Sepulcre J, Talukdar T, Krienen FM, Liu H, Hedden T, Andrews-Hanna JR, Sperling RA, Johnson KA (2009) Cortical hubs revealed by intrinsic functional connectivity: mapping, assessment of stability, and relation to Alzheimer's disease. J Neurosci 29(6):1860–1873

Busatto GF, Garrido GE, Almeida OP, Castro CC, Camargo CH, Cid CG, Buchpiguel CA, Furuie S, Bottino CM (2003) A voxel-based morphometry study of temporal lobe gray matter reductions in Alzheimer's disease. Neurobiol Aging 24(2):221–231

Caspers S, Geyer S, Schleicher A, Mohlberg H, Amunts K, Zilles K (2006) The human inferior parietal cortex: cytoarchitectonic parcellation and interindividual variability. NeuroImage 33(2):430–448

Caspers S, Eickhoff SB, Geyer S, Scheperjans F, Mohlberg H, Zilles K, Amunts K (2008) The human inferior parietal lobule in stereotaxic space. Brain Struct Funct 212(6):481–495

Caspers S, Eickhoff SB, Rick T, von Kapri A, Kuhlen T, Huang R, Shah NJ, Zilles K (2011) Probabilistic fibre tract analysis of cytoarchitectonically defined human inferior parietal lobule areas reveals similarities to macaques. NeuroImage 58(2):362–380

Caspers S, Schleicher A, Bacha-Trams M, Palomero-Gallagher N, Amunts K, Zilles K (2013) Organization of the human inferior parietal lobule based on receptor architectonics. Cereb Cortex 23(3):615–628

Cavada C, Goldman-Rakic PS (1989a) Posterior parietal cortex in rhesus monkey: I. Parcellation of areas based on distinctive limbic and sensory corticocortical connections. J Comp Neurol 287(4):393–421

Cavada C, Goldman-Rakic PS (1989b) Posterior parietal cortex in rhesus monkey: II. Evidence for segregated corticocortical networks linking sensory and limbic areas with the frontal lobe. J Comp Neurol 287(4):422–445

Chai XJ, Castanon AN, Ongur D, Whitfield-Gabrieli S (2012) Anticorrelations in resting state networks without global signal regression. Neuroimage 59(2):1420–1428

Crone EA, Wendelken C, Donohue SE, Bunge SA (2006) Neural evidence for dissociable components of task-switching. Cereb Cortex 16(4):475–486

Dai W, Lopez OL, Carmichael OT, Becker JT, Kuller LH, Gach HM (2009) Mild cognitive impairment and alzheimer disease:

patterns of altered cerebral blood flow at MR imaging. Radiology 250(3):856–866

Dai Z, Yan C, Wang Z, Wang J, Xia M, Li K, He Y (2012) Discriminative analysis of early Alzheimer's disease using multi-modal imaging and multi-level characterization with multi-classifier (M3). NeuroImage 59(3):2187–2195

Desikan RS, Cabral HJ, Fischl B, Guttmann CR, Blacker D, Hyman BT, Albert MS, Killiany RJ (2009) Temporoparietal MR imaging measures of atrophy in subjects with mild cognitive impairment that predict subsequent diagnosis of Alzheimer disease. Ajnr 30(3):532–538

Dickerson BC, Sperling RA (2009) Large-scale functional brain network abnormalities in Alzheimer's disease: insights from functional neuroimaging. Behav Neurol 21(1):63–75

Dosenbach NU, Fair DA, Miezin FM, Cohen AL, Wenger KK, Dosenbach RA, Fox MD, Snyder AZ, Vincent JL, Raichle ME, Schlaggar BL, Petersen SE (2007) Distinct brain networks for adaptive and stable task control in humans. Proc Natl Acad Sci USA 104(26):11073–11078

Downar J, Crawley AP, Mikulis DJ, Davis KD (2002) A cortical network sensitive to stimulus salience in a neutral behavioral context across multiple sensory modalities. J Neurophysiol 87(1):615–620

Dubois B, Feldman HH, Jacova C, Dekosky ST, Barberger-Gateau P, Cummings J, Delacourte A, Galasko D, Gauthier S, Jicha G, Meguro K, O'Brien J, Pasquier F, Robert P, Rossor M, Salloway S, Stern Y, Visser PJ, Scheltens P (2007) Research criteria for the diagnosis of Alzheimer's disease: revising the NINCDS-ADRDA criteria. Lancet Neurol 6(8):734–746

Dubois B, Feldman HH, Jacova C, Cummings JL, Dekosky ST, Barberger-Gateau P, Delacourte A, Frisoni G, Fox NC, Galasko D, Gauthier S, Hampel H, Jicha GA, Meguro K, O'Brien J, Pasquier F, Robert P, Rossor M, Salloway S, Sarazin M, de Souza LC, Stern Y, Visser PJ, Scheltens P (2010) Revising the definition of Alzheimer's disease: a new lexicon. Lancet Neurol 9(11):1118–1127

Eickhoff SB, Stephan KE, Mohlberg H, Grefkes C, Fink GR, Amunts K, Zilles K (2005) A new SPM toolbox for combining probabilistic cytoarchitectonic maps and functional imaging data. NeuroImage 25(4):1325–1335

Fox MD, Zhang D, Snyder AZ, Raichle ME (2009) The global signal and observed anticorrelated resting state brain networks. J Neurophysiol 101(6):3270–3283

Frisoni GB, Testa C, Zorzan A, Sabattoli F, Beltramello A, Soininen H, Laakso MP (2002) Detection of grey matter loss in mild Alzheimer's disease with voxel based morphometry. J Neurol Neurosurg Psychiatry 73(6):657–664

Grady CL, McIntosh AR, Beig S, Keightley ML, Burian H, Black SE (2003) Evidence from functional neuroimaging of a compensatory prefrontal network in Alzheimer's disease. J Neurosci 23(3):986–993

Greene SJ, Killiany RJ (2010) Subregions of the inferior parietal lobule are affected in the progression to Alzheimer's disease. Neurobiol Aging 31(8):1304–1311

Gregoriou GG, Borra E, Matelli M, Luppino G (2006) Architectonic organization of the inferior parietal convexity of the macaque monkey. J Comp Neurol 496(3):422–451

Greicius MD, Srivastava G, Reiss AL, Menon V (2004) Default-mode network activity distinguishes Alzheimer's disease from healthy aging: evidence from functional MRI. Proc Natl Acad Sci USA 101(13):4637–4642

Guo X, Wang Z, Li K, Li Z, Qi Z, Jin Z, Yao L, Chen K (2010) Voxel-based assessment of gray and white matter volumes in Alzheimer's disease. Neurosci Lett 468(2):146–150

Hampson M, Driesen N, Roth JK, Gore JC, Constable RT (2010) Functional connectivity between task-positive and task-negative brain areas and its relation to working memory performance. Magn Reson Imaging 28(8):1051–1057

Hanakawa T, Dimyan MA, Hallett M (2008) Motor planning, imagery, and execution in the distributed motor network: a time-course study with functional MRI. Cereb Cortex 18(12):2775–2788

Hanyu H, Kume K, Sato T, Hirao K, Kanetaka H, Sakurai H, Iwamoto T (2012) Regional differences in cortical benzodiazepine receptors of Alzheimer, vascular, and mixed dementia patients. J Neurol Sci 323(1–2):71–76

Hao J, Li K, Li K, Zhang D, Wang W, Yang Y, Yan B, Shan B, Zhou X (2005) Visual attention deficits in Alzheimer's disease: an fMRI study. Neurosci Lett 385(1):18–23

He Y, Wang L, Zang Y, Tian L, Zhang X, Li K, Jiang T (2007) Regional coherence changes in the early stages of Alzheimer's disease: a combined structural and resting-state functional MRI study. NeuroImage 35(2):488–500

Iacoboni M (2005) Neural mechanisms of imitation. Curr Opin Neurobiol 15(6):632–637

Jacobs HI, Van Boxtel MP, Uylings HB, Gronenschild EH, Verhey FR, Jolles J (2011) Atrophy of the parietal lobe in preclinical dementia. Brain Cogn 75(2):154–163

Jacobs HI, Van Boxtel MP, Heinecke A, Gronenschild EH, Backes WH, Ramakers IH, Jolles J, Verhey FR (2012) Functional integration of parietal lobe activity in early Alzheimer disease. Neurology 78(5):352–360

Jenkinson M, Bannister P, Brady M, Smith S (2002) Improved optimization for the robust and accurate linear registration and motion correction of brain images. NeuroImage 17(2):825–841

Johannsen P, Jakobsen J, Bruhn P, Gjedde A (1999) Cortical responses to sustained and divided attention in Alzheimer's disease. NeuroImage 10(3 Pt 1):269–281

Kemppainen N, Ruottinen H, Nagren K, Rinne JO (2000) PET shows that striatal dopamine D1 and D2 receptors are differentially affected in AD. Neurology 55(2):205–209

Keysers C, Gazzola V (2009) Expanding the mirror: vicarious activity for actions, emotions, and sensations. Curr Opin Neurobiol 19(6):666–671

Lai MK, Tsang SW, Alder JT, Keene J, Hope T, Esiri MM, Francis PT, Chen CP (2005) Loss of serotonin 5-HT2A receptors in the postmortem temporal cortex correlates with rate of cognitive decline in Alzheimer's disease. Psychopharmacology 179(3):673–677

Laureys G, Clinckers R, Gerlo S, Spooren A, Wilczak N, Kooijman R, Smolders I, Michotte Y, De Keyser J (2010) Astrocytic beta(2)-adrenergic receptors: from physiology to pathology. Prog Neurobiol 91(3):189–199

Ledberg A, Akerman S, Roland PE (1998) Estimation of the probabilities of 3D clusters in functional brain images. NeuroImage 8(2):113–128

Liang P, Wang Z, Yang Y, Jia X, Li K (2011) Functional disconnection and compensation in mild cognitive impairment: evidence from DLPFC connectivity using resting-state fMRI. PLoS One 6(7):e22153

Limon A, Reyes-Ruiz JM, Miledi R (2012) Loss of functional GABA(A) receptors in the Alzheimer diseased brain. Proc Natl Acad Sci USA 109(25):10071–10076

Makris N, Kennedy DN, McInerney S, Sorensen AG, Wang R, Caviness VS Jr, Pandya DN (2005) Segmentation of subcomponents within the superior longitudinal fascicle in humans: a quantitative, in vivo. DT-MRI study. Cereb Cortex 15(6):854–869

Mars RB, Jbabdi S, Sallet J, O'Reilly JX, Croxson PL, Olivier E, Noonan MP, Bergmann C, Mitchell AS, Baxter MG, Behrens TE, Johansen-Berg H, Tomassini V, Miller KL, Rushworth MF (2011) Diffusion-weighted imaging tractography-based parcellation of

the human parietal cortex and comparison with human and macaque resting-state functional connectivity. J Neurosci 31(11):4087–4100

Medeiros R, Kitazawa M, Caccamo A, Baglietto-Vargas D, Estrada-Hernandez T, Cribbs DH, Fisher A, LaFerla FM (2011) Loss of muscarinic M1 receptor exacerbates Alzheimer's disease-like pathology and cognitive decline. Am J Pathol 179(2):980–991

Mishizen-Eberz AJ, Rissman RA, Carter TL, Ikonomovic MD, Wolfe BB, Armstrong DM (2004) Biochemical and molecular studies of NMDA receptor subunits NR1/2A/2B in hippocampal subregions throughout progression of Alzheimer's disease pathology. Neurobiol Dis 15(1):80–92

Morris JC (1993) The clinical dementia rating (CDR): current version and scoring rules. Neurology 43(11):2412–2414

Murphy K, Birn RM, Handwerker DA, Jones TB, Bandettini PA (2009) The impact of global signal regression on resting state correlations: are anti-correlated networks introduced? NeuroImage 44(3):893–905

Nelson PT, Abner EL, Scheff SW, Schmitt FA, Kryscio RJ, Jicha GA, Smith CD, Patel E, Markesbery WR (2009) Alzheimer's-type neuropathology in the precuneus is not increased relative to other areas of neocortex across a range of cognitive impairment. Neurosci Lett 450(3):336–339

Pariente J, Cole S, Henson R, Clare L, Kennedy A, Rossor M, Cipoloti L, Puel M, Demonet JF, Chollet F, Frackowiak RS (2005) Alzheimer's patients engage an alternative network during a memory task. Ann Neurol 58(6):870–879

Peeters R, Simone L, Nelissen K, Fabbri-Destro M, Vanduffel W, Rizzolatti G, Orban GA (2009) The representation of tool use in humans and monkeys: common and uniquely human features. J Neurosci 29(37):11523–11539

Pievani M, de Haan W, Wu T, Seeley WW, Frisoni GB (2011a) Functional network disruption in the degenerative dementias. Lancet Neurol 10(9):829–843

Pievani M, Galluzzi S, Thompson PM, Rasser PE, Bonetti M, Frisoni GB (2011b) APOE4 is associated with greater atrophy of the hippocampal formation in Alzheimer's disease. NeuroImage 55(3):909–919

Power JD, Barnes KA, Snyder AZ, Schlaggar BL, Petersen SE (2012) Spurious but systematic correlations in functional connectivity MRI networks arise from subject motion. NeuroImage 59(3):2142–2154

Proctor DT, Coulson EJ, Dodd PR (2011) Post-synaptic scaffolding protein interactions with glutamate receptors in synaptic dysfunction and Alzheimer's disease. Prog Neurobiol 93(4):509–521

Rushworth MF, Behrens TE, Johansen-Berg H (2006) Connection patterns distinguish 3 regions of human parietal cortex. Cereb Cortex 16(10):1418–1430

Sabbagh MN, Shah F, Reid RT, Sue L, Connor DJ, Peterson LK, Beach TG (2006) Pathologic and nicotinic receptor binding differences between mild cognitive impairment, Alzheimer disease, and normal aging. Arch Neurol 63(12):1771–1776

Satterthwaite TD, Wolf DH, Loughead J, Ruparel K, Elliott MA, Hakonarson H, Gur RC, Gur RE (2012) Impact of in-scanner head motion on multiple measures of functional connectivity: relevance for studies of neurodevelopment in youth. NeuroImage 60(1):623–632

Seeley WW, Menon V, Schatzberg AF, Keller J, Glover GH, Kenna H, Reiss AL, Greicius MD (2007) Dissociable intrinsic connectivity networks for salience processing and executive control. J Neurosci 27(9):2349–2356

Seeley WW, Crawford RK, Zhou J, Miller BL, Greicius MD (2009) Neurodegenerative diseases target large-scale human brain networks. Neuron 62(1):42–52

Seidenberg M, Guidotti L, Nielson KA, Woodard JL, Durgerian S, Antuono P, Zhang Q, Rao SM (2009) Semantic memory activation in individuals at risk for developing Alzheimer disease. Neurology 73(8):612–620

Song XW, Dong ZY, Long XY, Li SF, Zuo XN, Zhu CZ, He Y, Yan CG, Zang YF (2011) REST: a toolkit for resting-state functional magnetic resonance imaging data processing. PLoS One 6(9):e25031

Truchot L, Costes N, Zimmer L, Laurent B, Le Bars D, Thomas-Anterion C, Mercier B, Hermier M, Vighetto A, Krolak-Salmon P (2008) A distinct [18F]MPPF PET profile in amnestic mild cognitive impairment compared to mild Alzheimer's disease. NeuroImage 40(3):1251–1256

Uddin LQ, Supekar KS, Ryali S, Menon V (2011) Dynamic reconfiguration of structural and functional connectivity across core neurocognitive brain networks with development. J Neurosci 31(50):18578–18589

Van Dijk KR, Sabuncu MR, Buckner RL (2012) The influence of head motion on intrinsic functional connectivity MRI. NeuroImage 59(1):431–438

Vidoni ED, Thomas GP, Honea RA, Loskutova N, Burns JM (2012) Evidence of altered corticomotor system connectivity in early-stage Alzheimer's disease. J Neurol Phys Ther: JNPT 36(1):8–16

Vincent JL, Kahn I, Snyder AZ, Raichle ME, Buckner RL (2008) Evidence for a frontoparietal control system revealed by intrinsic functional connectivity. J Neurophysiol 100(6):3328–3342

Walhovd KB, Fjell AM, Brewer J, McEvoy LK, Fennema-Notestine C, Hagler DJ Jr, Jennings RG, Karow D, Dale AM (2010) Combining MR imaging, positron-emission tomography, and CSF biomarkers in the diagnosis and prognosis of Alzheimer disease. Ajnr 31(2):347–354

Wang L, Zang Y, He Y, Liang M, Zhang X, Tian L, Wu T, Jiang T, Li K (2006) Changes in hippocampal connectivity in the early stages of Alzheimer's disease: evidence from resting state fMRI. NeuroImage 31(2):496–504

Wang K, Liang M, Wang L, Tian L, Zhang X, Li K, Jiang T (2007) Altered functional connectivity in early Alzheimer's disease: a resting-state fMRI study. Hum Brain Mapp 28(10):967–978

Wang Z, Yan C, Zhao C, Qi Z, Zhou W, Lu J, He Y, Li K (2011) Spatial patterns of intrinsic brain activity in mild cognitive impairment and Alzheimer's disease: a resting-state functional MRI study. Hum Brain Mapp 32:1720–1740

Wang J, Fan L, Zhang Y, Liu Y, Jiang D, Zhang Y, Yu C, Jiang T (2012a) Tractography-based parcellation of the human left inferior parietal lobule. NeuroImage 63(2):641–652

Wang Z, Jia X, Liang P, Qi Z, Yang Y, Zhou W, Li K (2012b) Changes in thalamus connectivity in mild cognitive impairment: evidence from resting state fMRI. Eur J Radiol 81:277–285

Wang J, Zuo X, Dai Z, Xia M, Zhao Z, Zhao X, Jia J, Han Y, He Y (2013) Disrupted functional brain connectome in individuals at risk for Alzheimer's disease. Biol Psychiatry 73(5):472–481

Weissenbacher A, Kasess C, Gerstl F, Lanzenberger R, Moser E, Windischberger C (2009) Correlations and anticorrelations in resting-state functional connectivity MRI: a quantitative comparison of preprocessing strategies. NeuroImage 47(4):1408–1416

Xia M, Wang J, He Y (2013) BrainNet Viewer: a network visualization tool for human brain connectomics. PLoS One 8(7):e68910. doi:10.1371/journal.pone.0068910

Xiong H, McCabe L, Costello J, Anderson E, Weber G, Ikezu T (2004) Activation of NR1a/NR2B receptors by soluble factors from APP-stimulated monocyte-derived macrophages: implications for the pathogenesis of Alzheimer's disease. Neurobiol Aging 25(7):905–911

Xu Y, Yan J, Zhou P, Li J, Gao H, Xia Y, Wang Q (2012) Neurotransmitter receptors and cognitive dysfunction in

Alzheimer's disease and Parkinson's disease. Prog Neurobiol 97(1):1–13

Yan C, Zang Y (2010) DPARSF: a MATLAB toolbox for "Pipeline" data analysis of resting-state fMRI. Front Syst Neurosci 4:13

Zhang D, Raichle ME (2010) Disease and the brain's dark energy. Nat Rev Neurol 6(1):15–28

Zhang HY, Wang SJ, Liu B, Ma ZL, Yang M, Zhang ZJ, Teng GJ (2010) Resting brain connectivity: changes during the progress of Alzheimer disease. Radiology 256(2):598–606

Zilles K, Amunts K (2010) Centenary of Brodmann's map—conception and fate. Nat Rev Neurosci 11(2):139–145

Zuo XN, Kelly C, Di Martino A, Mennes M, Margulies DS, Bangaru S, Grzadzinski R, Evans AC, Zang YF, Castellanos FX, Milham MP (2010) Growing together and growing apart: regional and sex differences in the lifespan developmental trajectories of functional homotopy. J Neurosci 30(45):15034–15043